JOURNAL OF KUFA–PHYSICS
journal.uokufa.edu.iq/index.php/jkp/index | ISSN: 2077–5830

# Enhancing the Sensitivity of Silver Oxide Sensors to $NO_2$ Gas by Adding a TFB Polymer

**Zainab Ali Qatea[1*] & Omar Adnan Ibrabim[2]**

*[1,2]Department of Physics, College of Science, University of Baghdad, Baghdad, Iraq*

*[*]Corresponding Author E-mail: zainab.ali2304@sc.uobaghdad.edu.iq*

**ARTICLE INF.**

***Article history:***
Received: 22 SEP., 2025
Revised: 12 NOV., 2025
Accepted: 24 NOV., 2025
Available Online: 27 DEC. 2025

***Keywords:***

Silver oxide

TFB polymer

Pulsed laser deposition

$NO_2$ gas sensor

Gas sensitivity

Nanostructured thin films

**ABSTRACT**

In this study, a poly[(9,9-dioctylfluorenyl-2,7-diyl)-co-(4,4′-(N-(4-sec-butylphenyl) diphenylamine))] (TFB) polymer was added to silver oxide (AgO) thin films to increase their sensitivity. The S2 (TFB/AgO) sample demonstrated the highest sensitivity of 172.6% at an operating temperature of 150 °C and the shortest recovery time of 6 s at 25 °C and 200 °C. The composite films showed the biggest change in electrical resistance. Pulsed laser deposition (PLD) was used to deposit AgO thin films on glass and quartz substrates, and spin coating was used to deposit TFB polymer layers to create uniform films. AgO has a polycrystalline cubic structure, and the addition of TFB did not change this crystal structure, according to X-ray diffraction (XRD) analysis, which verified that TFB is amorphous. The TFB/AgO sample displayed dominant AgO absorption in the optical absorption spectra, while the polymer encasing the AgO particles made TFB absorption more noticeable in the TFB:AgO mixed film. Both AgO and TFB were identified by Fourier-transform infrared (FTIR) analysis, which showed distinct absorption peaks with observable shifts and intensity variations in the composite samples. The interaction between TFB and AgO and the creation of altered interfacial bonds are confirmed by these spectral shifts.

DOI: https://doi.org/10.31257/2018/JKP/2025/v17.i02.21566

# تعزيز حساسية متحسسات أوكسيد الفضة لغاز $NO_2$ بإضافة بوليمر TFB

**زينب علي كاطع[1]. عمر عدنان إبراهيم[2]**

[1,2]قسم الفيزياء، كلية العلوم، جامعة بغداد، بغداد، العراق

**الكلمات المفتاحية:**

أوكسيد الفضة
بوليمر TFB
الترسيب بالليزر النبضي
متحسس غاز $NO_2$

**الـــخُـــلاصـــة**

في هذه الدراسة، تم إضافة بوليمر poly[(9,9-dioctylfluorenyl-2,7-diyl)-co-(4,4′-(N-(4-sec-butylphenyl)diphenylamine))] (TFB) إلى أغشية رقيقة من أكسيد الفضة (AgO) لزيادة حساسيتها. أظهر عينة (TFB/AgO) أعلى حساسية بنسبة 172.6% عند درجة حرارة تشغيل تبلغ 150 °م وأقصر زمن للتعافي قدره 6 ثوانٍ عند 25 °م و200 °م. وأظهرت الأغشية

المركبة أكبر تغير في المقاومة الكهربائية. تم استخدام طريقة الترسيب بالليزر النبضي (PLD) لترسيب الأغشية الرقيقة من AgO على ركائز من الزجاج والكوارتز، وتم استخدام الطلاء بالدوران لترسيب طبقات البوليمر TFB لإنشاء أغشية متجانسة. يمتلك AgO بنية مكعبة متعددة البلورات، ولم يغير إضافة TFB هذه البنية البلورية، وفقًا لتحليل حيود الأشعة السينية (XRD)، الذي أكد أن TFB غير متبلور. في أطياف الامتصاص الضوئي، أظهرت عينة TFB/AgO امتصاص AgO السائد، بينما في الفيلم المختلط TFB:AgO أصبح امتصاص TFB أكثر بروزًا بسبب تغليف البوليمر لجزيئات AgO. تم تحديد كل من AgO و TFBبواسطة تحليل التحليل الطيفي بالأشعة تحت الحمراء لتحويل فوريه(FTIR)، والذي أظهر قمم امتصاص مميزة مع تحولات ملحوظة وتغيرات في الشدة في العينات المركبة. يتم تأكيد التفاعل بين TFB و AgOوخلق روابط واجهة معدلة من خلال هذه التحولات الطيفية.

متحسس غاز

## 1. INTRODUCTION

Environment is the most important concern in a human life and any change in it affect our lives significantly. Thus, a special attention and must be payed, especially, when using an extraordinary amount of fossil fuels. These activities affect the purity of the air directly and for this reason that see recently the air pollution has become a major global concern that can result in major health issues [1]. In addition to the ecosystem, it has become necessary to identify and detect gas molecules in the air at low concentrations in many areas such as environmental monitoring, public security, as well as food safety, medical and military diagnostics [2-4]. The atmospheric air people breathe consists of about 78% nitrogen ($N_2$), 21% oxygen ($O_2$) and 0.9% argon (Ar), carbon dioxide ($CO_2$) by 0.03% and other gases by 0.07%. But, there are many contaminants which impurifies the air and affect its quality such as NOx, (CO), $O_3$, and ($SO_2$) [5, 6]. $NO_2$ is one of the most dangerous and toxic gases, which strongly pollutes the atmosphere and has a negative effect on both humans and other living organisms [7-8]. Herein, the main contributor in acidic rains is the (NOx) due to the interaction between this gas with the vapor before the precipitation. Add to that the global warming and Ozone level which are related to $NO_2$. It also contributes to a number of nitration processes with biomolecules, which can lead to cancer and other asthmatic conditions in humans. From this point, effective sensors are necessary to trace the level of detection of NOx gas. At the same time, some features like the size, simpe configuration, and cost must be available in the sensor and it is worth mentioning these features that can be made in metal-oxide-based structure smoothly [9]. So, many researchers have focused on this type of sensors. For example, Composite materials have drawn a lot of attention lately because of their special blend of organic and inorganic qualities, as well as their useful qualities and numerous uses. [10] and organic matter used the poly [(9,9-dioctylfluorenyl-2,7-diyl)- co (4,4′-(N-(4-sec-butylphenyl) diphenylamine)],(TFB), is a fluorene copo-lymer with a molecular weight of approximately 80,000–120,000 g/mol, supplied by American Dye Source, Inc. The conjugated polymer (TFB) was selected for its chemical stability, good film-forming ability, and its ability to enhance charge transfer and improve film uniformity [11]. where they used

some practical strategies including spin coating technique [12]. To enhance the performance of the gas sensors of metal-oxide-based structured, the surface to volume ratio must be high enough to detect the low concentrations. This condition can be reached when the sensor is made based on the nanostructured layers configuration. This kind of structure has high performance and accuracy in terms of gas sensors [13-14]. AgO was selected as a sensing material due to its strong chemical reactivity toward oxidizing gases like $NO_2$, wide band gap (1.2–3.4 eV), and good electrical conductivity [15–17].

Previous studies mainly focused on other metal oxides such as ZnO, $SnO_2$, and $TiO_2$ for $NO_2$ detection, while limited work has been reported on AgO combined with polymers. In order to bridge this gap, this work uses TFB polymer with AgO to increase the sensitivity and stability of $NO_2$ gas sensors. In this study, the effect of adding the TFB polymer deposited by spin coating to silver oxide AgO deposited by pulsed laser deposition on quartz and glass substrates was studied and the compositional and optical properties and sensitivity to toxic $NO_2$ gas at different operating temperatures were also studied.

## 2. Experimental Procedures

In this work, glass and quartz substrates were used, the substrates were cleaned using distilled water and ethanol alcohol and dried in oven, TFB was obtained from the American dye source company, Fig.1, shows the TFB planar molecular structural formula and the optimized geometric structure.

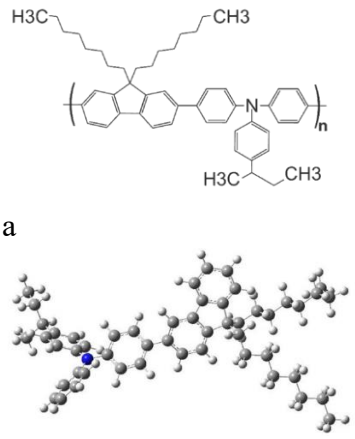


a

b

**Figure (1): (**a) Planar molecular structure, and (b)optimized geometric structure of TFB.

The TFB polymer solution was prepared by dissolving 0.62 mg in 4 ml of chloroform dissolved at room temperature (approximately 25 °C) , the solution was placed in a magnetic stirrer in order to dissolve the polymer well and then left in the dark overnight to complete the dissolution process.

The silver oxide tablet was prepared in the form of compressed 1cm and a thickness of 0.5 cm with a hydraulic press under pressure of 10 tons for 15 min. The samples were coded as indicated in Table 1.

The S1 sample was prepared first by depositing the aluminum electrodes on the substrate by thermal evaporation method with a thickness of 500 nm and then the TFB polymer was deposited by spin coating method, and the deposition was done at a speed of 1000 rpm, for 30 seconds, after which the sample was placed in the oven at a temperature of 60 ° C, for 30 min.

S2 sample, which consists of aluminum electrodes, TFB polymer and AgO, was prepared by depositing aluminum electrodes first on the

substrate by thermal evaporation method with a thickness of 500 nm and then TFB polymer was deposited on the electrodes using the spin coating method at a speed of 1000 rpm and a time of 30 seconds and was placed in the oven at a temperature of 60°C for30 minutes to dry complete, after that a layer of AgO was deposited on the polymer using the pulsed laser deposition method by Nd: YAG laser The deposition conditions were under a pressure of $1\times10^{-2}$ mbar, a frequency of 1Hz and (200) pulses, which is concentrated through a window to collide with the target (silver oxide disk). The material flows in a certain way and forward on the substrate and is deposited with the least pollution possible.

The S3 sample consisting of the AgO layer was prepared, as well as using the pulsed laser deposition method under a pressure of $1\times10^{-2}$ mbar, the frequency is 1 Hz and the number of pulses is 200 pulses, after which the aluminum electrodes were deposited on the AgO layer by thermal evaporation method with a thickness of 500 nm.

In order to prepare the sample S4, sample S2 was redeposited with the same steps mentioned earlier, after which the polymer and silver oxide layers were dissolved using 3 ml of chloroform in a glass vial, the solution was mixed with an ultrasonic probe device. Then the was deposited solution by spin coating method at a speed of 1000 rpm, for 30 sec and put in the oven at a temperature of 60 ° C for 30 min. All samples are shown in a diagram in Fig.2.

To determine the size and structure of the crystals, the samples were analyzed using X-ray diffraction. with Cu-Kα radiation (λ = 1.5405 Aº) (Redefining Benchtop XRD), The thickness and morphology of the deposited films were carefully characterized to evaluate their structural and surface properties. Were determined by Field Emission Scanning Electron Microscope (Inspect $^{TM}$ F50) device, the optical properties were examined using UV-Vis spectrophotometer model Lambda 365 Perkin Elmer in the wavelength range 190-1100nm double beam, Hall effect was measured using (Ecopia HMS-300).

**Table 1:** Code of the sample with the conditions for the preparation of thin films**.**

| Sample | Materials |
|---|---|
| S1 | TFB |
| S2 | TFB/AgO |
| S3 | AgO |
| S4 | TFB: AgO |

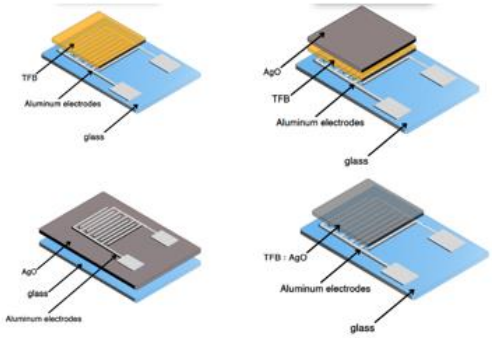


**Figure (2):** (a)S1-TFB, (b)S2-TFB/AgO, (c)S3-AgO, (d)S4-TFB: AgO

## 3. Results and Discussion

### *3.1 X-ray Diffraction*

X-ray diffraction (XRD) analysis was performed to investigate

the crystallite structure of the silver oxides and TFB polymer, as presented in Fig.3. The X-ray diffraction (XRD) analysis of the silver oxide (AgO) films prepared by the PLD method revealed distinct diffraction peaks at 2θ angles of 34.92°, 37.86°, 43.59°, 64.27°, and 77.12°, corresponding to the (002), (111), (012), (022), and (023), crystallographic planes, respectively (Fig.3. and Table 2). These peaks are consistent with the standard JCPDS card No. 43-1038 data and literature reports [17–20].

The amorphous nature of the polymer TFB and its thin layer over a glass substrate (quartz) typically result in a broad halo near 2θ ≈ 20° in the XRD patterns. The literature has extensive documentation on this phenomenon (Cullity & Stock 2001; Paul & Robeson 2008). [21].

The XRD pattern in the S4 (TFB:AgO composite) case is dominated by the broad amorphous halo of TFB, while AgO only exhibited a very weak reflection. This behavior is frequently observed in polymer/oxide nanocomposites, where the inorganic phase's crystallization is suppressed or limited by the amorphous polymer matrix. [22,23]. The same AgO diffraction peaks were seen at the same locations in S2 TFB/AgO and S1 AgO, but S2 peak intensities are lower. The growth of AgO on top of the TFB layer, where the underlying polymer functions as a seed layer and affects the crystallite orientation, is responsible for this reduction. Furthermore, this bilayer sample also exhibits a weak TFB peak [24]. From all these measurements, that did not notice any peak indicating structural interference between TFB and AgO. This means when mixing TFB with AgO no new peaks appeared. This is due to the fact that the diffraction angle for TFB is very far from the diffraction angle for AgO.

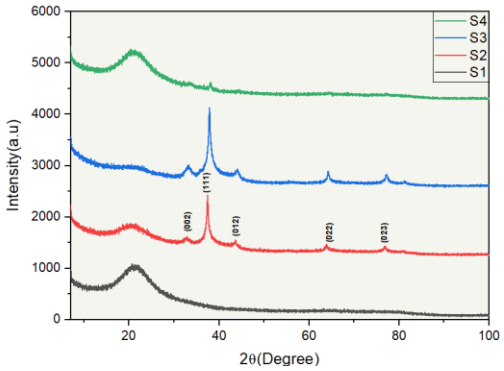


**Figure (3):** The XRD patterns of the deposited nano-silver oxide and TFB thin films.

XRD is crystallite size and lattice strain is a commonly used technique for figuring out a crystal's dimensional parameters and, more recently, for estimating the size of nanoparticles [25].

The average size of the crystals was calculated using the Debye-Scherrer equation as the mean value of all the main diffraction peaks for each sample from Eq. (1) [26].

$$D = \frac{K\lambda}{\beta_d \cos\theta} \qquad (1)$$

The shape factor is denoted by K varies between 0.89-1 depending upon crystal shape (K=0.9 in this work), the X-ray wavelength λ is usually 1.54 Å, the Bragg angle by θ, and the mean size of the ordered (crystallite) domains, D, may be smaller or equal to the grain size [25]. Table 2, shows the Crystallite size,

full width half maximum, angle and Miller coefficients.

**Table 2.** The diffraction angle, FWHM, size and the Miler indices of growing planes of the silver oxide thin films

| Sample No. | Crystallite size (nm) | 2θ (Deg.) | FWHM (Deg.) | h k l |
|---|---|---|---|---|
| S1 | ---------- | ---------- | ---------- | ---------- |
| S2 | 14.9 | 32.8 | 1.148 | (002) |
| | | 37.4 | 0.758 | (111) |
| | | 43.4 | 1.024 | (012) |
| | | 63.8 | 0.730 | (022) |
| | | 76.5 | 0.819 | (023) |
| S3 | 10.7 | 34.2 | 1.432 | (002) |
| | | 37.8 | 0.948 | (111) |
| | | 43.5 | 0.595 | (012) |
| | | 64.2 | 0.881 | (022) |
| | | 77.1 | 0.968 | (023) |
| S4 | 7.4 | 33.6 | 1.033 | (002) |
| | | 38.1 | 0.422 | (111) |

### *3.2 Cross-Sectional Analysis*

The cross-sectional FESEM images in Fig.4, clearly show the bilayer structure of TFB and AgO. Low contrast indicates a smooth transition rather than a distinct boundary at the interface between the polymer (TFB) and the oxide film. The energetic species in the pulsed laser deposition (PLD) process are responsible for this behavior. They may cause a small amount of intermixing at the interface, making a clear separation less visible [27]. Additionally, good film coverage and adhesion on the underlying TFB polymer are indicated by the uniformity of the AgO top layer, which has an average thickness of about 807 nm. According to the sum of the individual layers, the TFB/AgO bilayer's overall thickness was determined to be roughly 3.76 µm.

This demonstrates how the spin-coated TFB layer (2.95 µm) served as a stable foundation for the AgO deposition that followed. Since smooth interfaces are frequently desired for stable charge transport and gas diffusion pathways, the bilayer's compact morphology and continuous growth indicate that the chosen fabrication technique is dependable for sensor applications [28].

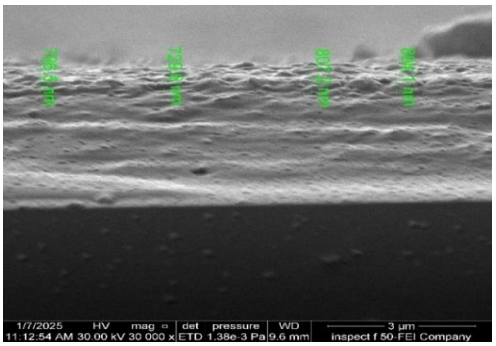

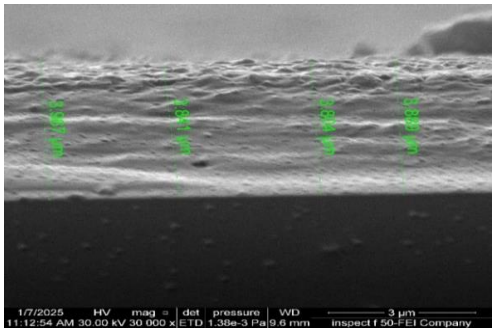

**Figure (4):** Cross Section for S2-TFB/AgO

### *3.3 UV-VIS Spectrophotometry*

The absorption spectra of all prepared samples are shown in Fig. 5 within the wavelength range of 200–1100 nm. In line with earlier research, the TFB polymer film (S1) exhibits a primary absorption peak at roughly 370 nm [12, 29]. Since AgO strongly absorbs light over the majority of the visible range and partially blocks the absorption of polymers, AgO dominates the absorption for the bilayer sample (S2, TFB/AgO) [30]. In the visible spectrum, the pure AgO film (S3) shows a strong absorption with a distinct feature between 400 and 500 nm. The primary absorption peak in the mixed composite (S4, TFB:AgO) reappears around 370 nm, suggesting that TFB encapsulates or covers the AgO particles, resulting in the polymer-absorption dominance.

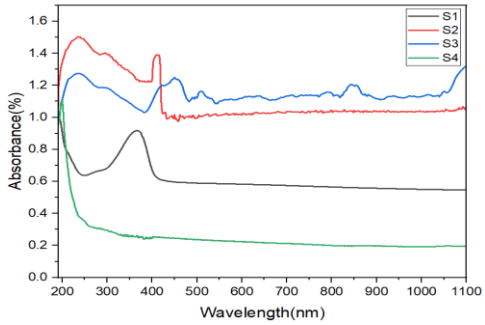


**Figure (5):** Normalized absorption spectra of the samples S1-TFB, S2-TFB/AgO, S3-AgO, S4-TFB: AgO

The optical absorption coefficient constant (α) has been determined Using the following Eq. (2).

$$\alpha = \frac{2.303A}{t} \qquad (2)$$

Where A is the absorbance and t are the thickness. Fig.6, show the fluctuation of $(\alpha h\upsilon)^2$ for TFB and AgO thin films as a function of photon energy gap. It should be mentioned that the absorption edge, not the absorption peak, is used to calculate the optical band gap for thin films. In this study, the absorption edge was determined using the absorption spectra in Fig.5, the band gap values listed in Table 3. Tauc's equation was used to evaluate the change of (αhυ)2 Eq. (3).

$$(\alpha h\upsilon) = A(h\upsilon - Eg)^n \qquad (3)$$

Where A is a constant that represents the absorption coefficient, (Eg) is the optical energy band gap, and (hv) is the input photon energy. The linear nature of the $(\alpha hv)^2$ versus (hv) plot indicates that the optical transitions in TFB, AgO, and composite films are direct allowed transitions. n = 1/2 was used for this equation's direct transition [31,32]. Table 3 shows the energy gap values for thin films composed of TFB and AgO.

**Table 3.** Values of the energy gap of the prepared thin films

| Simples | E.g. (eV) |
|---|---|
| S1-TFB | 2.96 |
| S2-TFB/AgO | 2.92 |
| S3-AgO | 2.52 |
| S4-TFB: AgO | 2.99 |

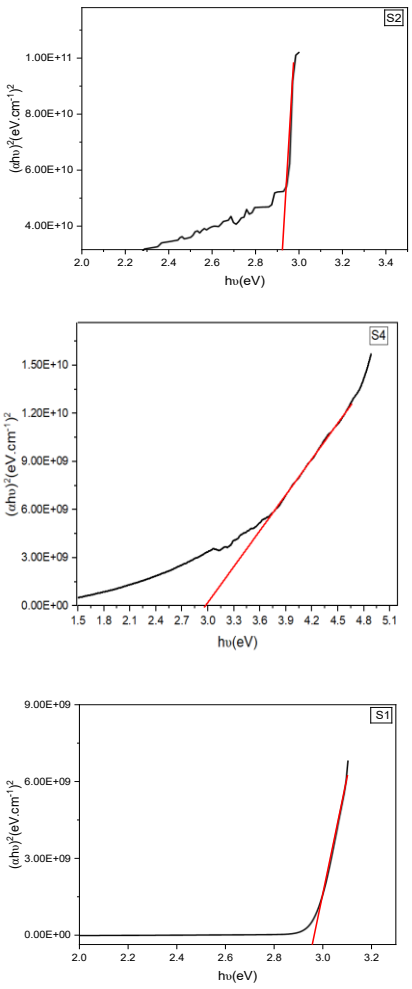


**Figure (6):** $[(\alpha h\nu)^{1/2}$ and $(\alpha h\nu)^{2}]$ versus photon energy (hν) for S1, S2, S3, S4

### *3.4 Fourier Transform-Infrared (FTIR)*

The TFB and AgO absorption spectra, as analyzed by FT-IR spectra, in wavenumber regions from 500 to 4,000 $cm^{-1}$. A certain wavelength of electromagnetic radiation is absorbed by organic matter while allowing other wavelengths to pass through. The molecular vibration property of infrared radiation can be used to determine the wavelength of absorption of organic matter and monitor the molecular structure of that substance. The molecular structure of AgO is shown in Fig.7. Peak wavenumbers in infrared materials exposed to infrared radiation in FT-IR analysis were previously reported in the results in Table 4. The TFB molecular structure is shown in Fig.7, Wavenumber peaks in organic materials exposed to infrared radiation in FT-IR analysis have been previously reported. 815 $cm^{-1}$ peaks were found to be due to C-H bending out-of-plane vibrations of para-disubstituted benzene rings; 1112 $cm^{-1}$ peaks were due to the bending mode of C-C stretching between phenylene rings or the C-H bending mode of the side chains. The 1288 $cm^{-1}$ peak appears to be the C-C stretching mode.

between phenylene rings, finally, the 1319 $cm^{-1}$ peak is the vibration peak of the C-H bends [29]. A band observed near 3425 $cm^{-1}$ corresponds to the O–H stretching vibration. Bands near 1632 $cm^{-1}$ are associated with O-H bending vibrations of adsorbed water molecules on the surface of silver oxide nanoparticles [33-36]. FTIR peaks observed in the range of 2853, 2924 $cm^{-1}$ of a thin film of AgO (silver oxide) are likely to correspond to C-H aldehyde expansion vibrations [37]. Moreover, bands at 1384 $cm^{-1}$ and 1465 $cm^{-1}$ are attributable to the $CO_2$ stretching [38,39], peak at 1114 $cm^{-1}$ is associated with Si–O–Si stretching vibrations originating from the substrate material, A characteristic absorption band at 618 $cm^{-1}$ corresponds to the stretching and bending vibrational modes of Ag–O bonds.

It was observed that the persistence in 1632 has increased in intensity in TFB/AgO and TFB: AgO, In the TFB: AgO sample, there are many changes in

the peaks, which means that in this case it becomes a shift in the peaks and this is due to a shift in the length of the bonds, This means that when TFB envelops AgO due to changes in electrostatics or manipulates the length of the bond.

**Table 4.** FTIR of absorption peaks for TFB and silver oxide films

| bond type | wavenumber ($cm^{-1}$) | Explain for main vibration peaks |
|---|---|---|
| O-H | 3425 | stretching |
| C-H | 2853, 2924 | stretching vibrations |
| O-H | 1632 | Bending vibrations |
| CO2 | 1384,1465 | stretching |
| C-H | 813 | out-of-plane vibration from 1,4-disubstituted benzene rings |
| C-H | 1112 | bending mode of side chains |
| C-C | 1270 | stretching modes between phenylene rings |
| C-H | 1319 | bending |
| Si–O–Si | 1114 | stretching vibrations |
| Ag-O | 618 | stretching and bending |

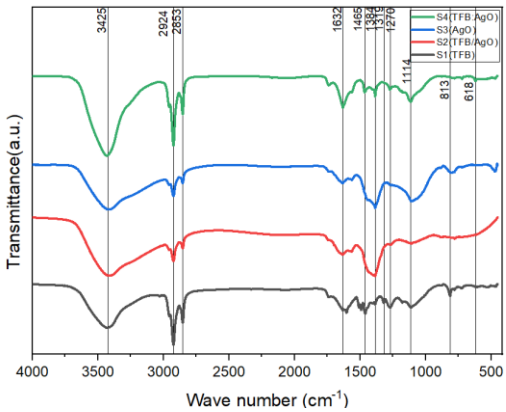


**Figure (7):** FTIR spectrum of silver oxide and TFB polymer thin film.

### *3.5 Gas Sensor Characteristics*

Measurements of gas sensing were carried out at a $NO_2$ concentration of 30 parts per million. Because pure TFB (sample S1) is chemically inert, it exhibited very little to no reaction at this concentration. TFB-based sensors can react to acetone (5% at 300 ppb), according to Chuang et al. (2018), but their sensitivity and selectivity are still restricted in practical settings. This implies that for gases like $NO_2$, TFB by itself might not be the best sensing material. But the bilayer TFB/AgO demonstrated a notable sensitivity, demonstrating AgO synergistic function in boosting gas reaction and charge transfer [40].

It is evident that the silver oxide/TFB compound has a much larger change in resistance between the maximum and minimum values than pure silver oxide, which has a higher sensitivity to $NO_2$ gas at an operating temperature of 100 °C (13.2), compared to the compound's higher sensitivity at an operating temperature of 150 °C (172.6). This is desirable because the noticeable change in resistance provides a clearer sensing signal. Small variations in resistance can be caused by preparation-related factors as well as external ones like wiring, temperature and contact resistance. These include microstrain, surface roughness, lattice defects, interfacial quality between the oxide and polymer layers. These elements were frequently found in PLD and spin-coated thin films, and they can affect charge transport and, in turn, the sensors' baseline resistance. Additionally, more symmetrical response-recovery curves are produced

by the addition of TFB polymer, suggesting enhanced stability and repeatability of the sensing behavior. A greater ΔR indicates a stronger interaction with gas molecules and, consequently, a higher sensitivity to toxic gases. This relationship between the magnitude of this change in resistance and the sensing signal has been documented in the literature [20,28].

An AgO and TFB mixing technique was used for sample S4. Although it was anticipated that the polymer would separate from AgO during spin coating deposition, the absence of any discernible sensing response in this work demonstrated that the two materials remained combined. The main goal of this mixing technique was to reduce the interfacial distance, which is around 10 nm and typically happens when the materials are deposited in different layers. The goal of this strategy was to enable possible energy transfer through interfacial contact by keeping AgO embedded and highly adherent within the TFB polymer. Nevertheless, no gas sensitivity was observed, which can be attributed to the encapsulation of AgO by the TFB polymer, suggesting that the layering method was more effective in this case.

A sensor's sensitivity (S) was determined by dividing the change in resistance by the value when the sensor's resistance value (Ra) in air is exposed to the target analyte. The microstructural and interfacial characteristics of the films are responsible for the variations in response and recovery times among the samples. In the TFB/AgO bilayer, the TFB polymer is essential for improving gas diffusion and charge transfer at the interface, and its high carrier mobility facilitates the quick transfer of charge to the AgO layer. Accordingly, the rapid recovery of 6 seconds at 25 °C and 200 °C indicates that the TFB layer improves both the gas absorption and release dynamics, Table 5 shows the sensitivity values, response time, and recovery time [41].

The following formula was used to determine the sensitivity from Eq. (4).

$$S\% = \frac{Rg-Ra}{Ra} \times 100\% \qquad (4)$$

where Ra is the resistance of the sensor in the air and Rg is the resistance of the sensor in the presence of $NO_2$ gas [43,44]. Fig.8, shows the sensitivity values for the prepared thin films.

**Table 5**: Response, recovery time and sensitivity of the TFB and AgO thin films exposed to $NO_2$ gas at room temperature.

| Sample No. | Temperature | Sensitivity(S %) | Response Time (sec) | Recovery Time (sec) |
|---|---|---|---|---|
| S1 | -------- | -------- | -------- | ------- |
| S2 | R.T | 16 | 43 | 6 |
| | 50 | 20.9 | 40 | 12 |
| | 100 | 167 | 13 | 9 |
| | 150 | 173 | 40 | 30 |
| | 200 | 07.9 | 5 | 6 |
| | R.T | 2.9 | 31 | 8 |

| | | | | |
|---|---|---|---|---|
| S3 | 50 | 3.7 | 17 | 29 |
| | 100 | 13.2 | 19 | 16 |
| | 150 | 18 | 28 | 30 |
| | 200 | 2.6 | 23 | 11 |
| S4 | -------- | -------- | -------- | -------- |

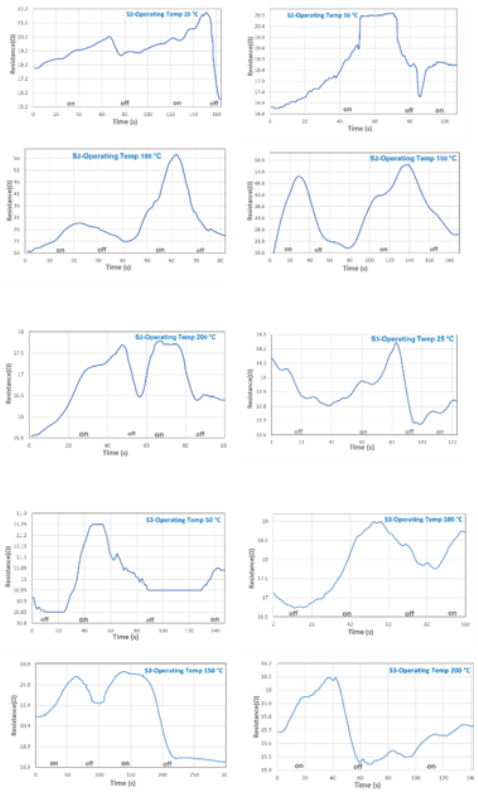

**Figure (8):** S2-TFB/AgO and S3-AgO thin film sensor resistance-time variation when exposed to $NO_2$ gas at R.T, 50, 100, 150, 200

## 4. Conclusions

PLD technology was used to deposit thin layers of AgO, and the polymer TFB was deposited by spin coating to create composite structures and bilayers. XRD technique confirmed the polycrystalline cubic phase of AgO and the amorphous nature of TFB. Depending on the layer composition, while cross-sectional images confirmed the layer thickness and the bilayer structures, optical studies revealed energy gap values ranging from 2.52 to 2.99 eV. The TFB/AgO bilayer (S2) showed better performance than pure AgO in gas sensing results, exhibiting the highest sensitivity to $NO_2$ at 172.6% at an operating temperature of 150°C with a fast response time of 6 seconds.

The TFB:AgO sample (S4) showed no response due to the TFB polymer encapsulating the AgO. These results indicate that combining AgO and TFB as layers enhances $NO_2$ gas sensing performance at relatively low temperatures.

## References

[1] S. Tyagi, M. Chaudhary, A. K. Ambedkar, K. Sharma, Y. K. Gautam, and B. P. Singh, "Metal oxide nanomaterial-based sensors for monitoring environmental $NO_2$ and its impact on the plant ecosystem: A review," *Sensors & Diagnostics*, Vol. 1, pp. 106–129, 2022.

[2] A. Bag and N. E. Lee, "Recent advances in development of transparent oxide semiconductor thin film transistors for flexible electronics," *J. Mater. Chem. C*, Vol. 7, pp. 13367–13383, 2019.

[3] R. Chauhan, N. Goel, M. Hojamberdiev, and M. Kumar, "Gas sensing properties of nanostructured metal oxide thin films," *Sens. Actuators A: Phys.*, Vol. 303, 111875, 2020.

[4] X. Liu, T. Ma, N. Pinna, and J. Zhang, "Two-dimensional

nanostructured materials for gas sensing applications," *Adv. Funct. Mater.*, Vol. 27, 1702168, 2017.

[5] R. J. Fiter, L. J. Murphy, M. N. Gong, and K. L. Cleven, "Advances in respiratory gas sensing technologies," *Expert Rev. Respir. Med.*, Vol. 17, pp. 1237–1247, 2023.

[6] M. V. Nikolic, V. Milovanovic, Z. Z. Vasiljevic, and Z. Stamenkovic, "Recent trends in gas sensors based on nanostructured metal oxides," *Sensors*, Vol. 20, 6694, 2020.

[7] T. Becker, S. Mühlberger, C. B. Braunmühl, G. Müller, T. Ziemann, and K. V. Hechtenberg, "Gas sensing with tin dioxide," *Sens. Actuators B: Chem.*, Vol. 69, pp. 108–119, 2000.

[8] A. Umar, A. A. Ibrahim, H. Algadi, H. Albargi, M. A. Alsairi, Y. Wang, and S. Akbar, "Nanostructured metal oxides for gas sensors," *Ceram. Int.*, Vol. 47, pp. 25696–25707, 2021.

[9] A. Sharma, M. Tomar, and V. Gupta, "$NO_2$ sensing properties of ZnO thin films," *Sens. Actuators B: Chem.*, Vol. 176, pp. 875–883, 2013.

[10] J. Huang, J. A. Moore, J. H. Acquaye, and R. B. Kaner, "Conducting polymers for gas sensing applications," *Macromolecules*, Vol. 38, pp. 317–321, 2005.

[11] W. Renzi, N. J. Cordeiro, H. de Santana, M. F. Costa, M. A. da Silva, E. Laureto, and J. L. Duarte, "Optical and structural properties of conducting polymers," *Synth. Met.*, Vol. 236, pp. 24–30, 2018.

[12] A. R. N. Rodrigues, W. Renzi, N. J. A. Cordeiro, E. Laureto, I. F. L. Dias, and J. L. Duarte, "Photoluminescence properties of polymer thin films," *Semina: Ciênc. Exatas Tecnol.*, Vol. 38, pp. 91–100, 2017.

[13] R. Jia, P. Xie, Y. Feng, Z. Chen, A. Umar, and Y. Wang, "Surface modification of nanostructured materials for gas sensing," *Appl. Surf. Sci.*, Vol. 440, pp. 409–414, 2018.

[14] S. K. Mustafa, L. A. Abdullah, K. A. Adam, and R. K. Jamal, "Optical properties of polymer-based thin films," *J. Optics*, pp. 1–8, 2024.

[15] S. Ravichandran, V. Paluria, G. Kumar, K. Loganathan, and B. R. K. Venkata, "Gas sensing using nanocomposite thin films," *J. Exp. Nanosci.*, Vol. 11, pp. 445–458, 2016.

[16] Z. H. Dhoondia and C. Hemlatta, "Synthesis of silver nanoparticles using fungi," *Nanomater. Nanotechnol.*, Vol. 2, pp. 15, 2012.

[17] H. H. Nayel and H. S. Al-Jumaili, "Characterization of silver oxide thin films prepared by chemical methods," *Iraqi J. Sci.*, Vol. 61, pp. 772–779, 2020.

[18] S. A. Irimiciuc, V. Grumezescu, A. M. Holban, O. Gherasim, S. Chertopalov, B. S. Vasile, P. Prepelita, V. Craciun, and J. Lancok, "Nanostructured polymer/oxide composites," *J. Appl. Phys.*, Vol. 136, pp. 1–10, 2024.

[19] N. R. C. Raju, K. J. Kumar, and A. Subrahmanyam, "Electrical and structural studies on silver oxide thin films," *J. Phys. D: Appl. Phys.*, Vol. 42, 135411, 2009.

[20] H. S. Ali, M. S. Sada, Y. I. Al-Rikabi, K. N. Hussein, N. F. Habubi, S. S. Chiad, and M. Jadan, "Optical and structural studies of silver oxide nanoparticles," *Dig. J. Nanomater. Biostruct.*, Vol. 19, pp. 513–520, 2024.

[21] D. R. Paul and L. M. Robeson, "Polymer nanocomposites: characterization and applications," *Polymer*, Vol. 49, pp. 3187–3204, 2008.

[22] B. D. Malhotra, A. Chaubey, and S. P. Singh, "Prospects of conducting polymers in biosensors," *Anal. Chim. Acta*, Vol. 578, pp. 59–74, 2006.

[23] Q. Zhao, F. Niu, J. Liu, and H. Yin, "Recent progress in polymer-based nanocomposites for sensors," *Polymers*, Vol. 16, 1899, 2024.

[24] Z. Yu, Y. Q. Li, F. Xia, and W. Xue, "Properties of silver oxide thin films prepared by reactive sputtering," *Surf. Coat. Technol.*, Vol. 204, pp. 131–134, 2009.

[25] H. R. Mohammed, "Synthesis and characterization of silver oxide thin films for gas sensing applications," M.Sc. thesis, University of Baghdad, 2019.

[26] V. D. Mote, Y. Purushotham, and B. N. Dole, "Williamson–Hall analysis in estimation of lattice strain in nanometer-sized ZnO particles," *J. Theor. Appl. Phys.*, Vol. 6, 6, 2012.

[27] R. Eason (ed.), *Pulsed Laser Deposition of Thin Films: Applications-Led Growth of Functional Materials*, John Wiley & Sons, 2006.

[28] E. Comini, G. Faglia, and G. Sberveglieri (eds.), *Solid State Gas Sensing*, Vol. 20, Springer, 2008.

[29] Y. J. Han, K. An, K. T. Kang, B. K. Ju, and K. H. Cho, "Highly sensitive $NO_2$ gas sensors using nanostructured thin films," *Sci. Rep.*, Vol. 9, 10385, 2019.

[30] T. O. Daniel and U. Nwankwo, "Optical properties of silver oxide thin films," *Rev. Mex. Fis.*, Vol. 71, 011003-1, 2025.

[31] O. A. Ibrahim, S. K. Mustafa, and R. K. Jamal, "Optical properties of AgO thin films prepared by PLD," *J. Optics*, pp. 1–5, 2024.

[32] H. H. Abbas and B. A. Hasan, "Structural and optical properties of silver oxide thin films," *Iraqi J. Sci.*, Vol. 63, pp. 1526–1539, 2022.

[33] S. Al-Zahrani, S. Astudillo-Calderón, B. Pintos, E. Pérez-Urria, J. A. Manzanera, L. Martín, and A. Gomez-Garay, "Applications of plant-based nanomaterials," *Plants*, Vol. 10, 1671, 2021.

[34] A. I. Oje, A. A. Ogwu, M. Mirzaeian, N. Tsendzughul, and A. M. Oje, "Electrical properties of silver oxide thin films," *J. Sci.: Adv. Mater. Devices*, Vol. 4, pp. 213–222, 2019.

[35] A. Rita, A. Sivakumar, S. S. J. Dhas, and S. M. B. Dhas, "Synthesis and characterization of nanostructured thin films," *J. Nanostruct. Chem.*, Vol. 10, pp. 309–316, 2020.

[36] A. S. Gungure, L. T. Jule, N. Nagaprasad, and K. Ramaswamy, "Nanocomposite thin film gas sensors," *Sci. Rep.*, Vol. 14, 26967, 2024.

[37] A. B. D. Nandiyanto, R. Oktiani, and R. Ragadhita, "How to read and write references in scientific papers," *Indones. J. Sci. Technol.*, Vol. 4, pp. 97–118, 2019.

[38] A. Sobhani-Nasab and M. Behpour, "Structural and optical properties of AgO thin films," *J. Mater. Sci.: Mater. Electron.*, Vol. 27, pp. 1191–1196, 2016.

[39] K. Kayed and B. Chiyah, "Aerosol deposition of oxide thin films," *Aerosol Sci. Eng.*, Vol. 4, pp. 271–276, 2020.

[40] M. Y. Chuang, Y. T. Lin, T. W. Tung, L. Y. Chang, H. W. Zan, H. F. Meng, C. J. Lu, and Y. T. Tao, "Room-temperature-operated organic-based acetone gas sensor for breath analysis," *Sens. Actuators B: Chem.*, Vol. 260, pp. 593–600, 2018.

[41] L. Y. Ng, A. W. Mohammad, C. P. Leo, and N. Hilal, "Polymeric membranes for water desalination," *Desalination*, Vol. 308, pp. 15–33, 2013.

[42] N. A. Abd and O. A. Ibrahim, "Optical properties of silver oxide thin films deposited by PLD," *Iraqi J. Phys.*, Vol. 22, pp. 1–10, 2024.

[43] H. J. Abaul-Ameer, M. F. Al-Hilli, and F. T. Ibrahim, "Structural and optical characterization of silver oxide thin films," *Iraqi J. Sci.*, Vol. 64, pp. 630–642, 2023.